

# Pulsed Laser Synthesis of SnO<sub>2</sub>-Pt Nano-Thin Films onto Carbon Nanotubes and their Electrocatalytic Activity Towards Ethanol Oxidation

Amel Tabet-Aoul<sup>1</sup>, Fatma Saidani<sup>1</sup>, Dominic Rochefort<sup>2</sup> and Mohamed Mohamedi<sup>1,\*</sup>

<sup>1</sup>Institut National de la Recherche Scientifique (INRS)-Énergie, Matériaux et Télécommunications (EMT), 1650 Boulevard Lionel Boulet, Varennes, Québec, J3X 1S2, Canada.

<sup>2</sup>Department of Chemistry, University of Montreal, CP 6128 Centre-Ville, Montreal Québec, H3C 3J7, Canada

\*E-mail: [mohamedi@emt.inrs.ca](mailto:mohamedi@emt.inrs.ca)

*Received:* 8 September 2011 / *Accepted:* 29 October 2011 / *Published:* 1 December 2011

---

In this work, we report the synthesis and characterization of nanoscaled CNT/SnO<sub>2</sub>/Pt films. The SnO<sub>2</sub> and Pt films were deposited using the pulsed laser deposition technique. Films of nanometric thicknesses of 17 nm and 40 nm for SnO<sub>2</sub> and Pt, respectively were obtained. SEM, TEM and XPS analysis all confirmed that each film was evenly coating the layer underneath, i.e., Pt onto SnO<sub>2</sub> onto CNTs. Pt was chosen as a benchmark catalyst to evaluate the electrocatalytic behavior of such structures. Thus, electrochemical tests have shown that CNT/SnO<sub>2</sub>/Pt nanoscaled structures displayed good electrocatalytic activity and stability when used as anode for ethanol electro-oxidation.

---

**Keywords:** Tin dioxide; platinum; carbon nanotubes; scaled nanofilms; ethanol electro-oxidation

## 1. INTRODUCTION

Tin dioxide is an excellent candidate for a wide range of applications such as transparent conducting electrodes [1], solid-state gas sensors [2-3], lithium-ion batteries[4], supercapacitors [5], solar cells [6-7], and alcohol fuel cells [8-10].

In ethanol electrooxidation mechanism at Pt/SnO<sub>2</sub> electrodes, SnO<sub>2</sub>'s role is believed to provide OH to oxidize strongly bound intermediates, such as CO [11-12]. Very little work has been devoted to the synthesis of Pt/SnO<sub>2</sub> materials and the investigation of their electrocatalytic properties towards ethanol oxidation.

Higuchi et al. prepared nafion-coated Pt/SnO<sub>2</sub> electrodes made of dispersed Pt and SnO<sub>2</sub> double nanoparticles containing different Pt/Sn ratios on carbon black (CB) by the modified Bönemann

method [13]. The authors showed that Pt/SnO<sub>2</sub>(3:1)/CB electrode displays the highest specific activity and lowest overpotential for ethanol oxidation reaction (EOR), and was superior to a Pt/CB electrode. By means of the hydrothermal method, Zhang et al. first synthesized SnO<sub>2</sub> nanoflowers and nanorods and then Pt/SnO<sub>2</sub> catalysts were chemically prepared from a mixture of the SnO<sub>2</sub> nanocrystals and H<sub>2</sub>PtCl<sub>6</sub>·6H<sub>2</sub>O and the whole was casted onto graphite support using nafion solution as a binder [14]. The authors found that Pt nanoparticles on the SnO<sub>2</sub> flowers exhibit a highly catalytic oxidation activity ethanol in acid solution. Giancarlo R. Salazar-Banda et al. prepared boron-doped diamond (BDD) film surfaces modified with Pt, Pt–SnO<sub>2</sub> nano-crystalline deposits by the sol–gel method. The authors reports an enhanced catalytic performance for ethanol oxidation with the Pt–SnO<sub>2</sub>/BDD electrode compared to Pt/BDD electrode [15]. Hsu et al. prepared SnO<sub>2</sub>-coated single-walled carbon nanotube (SWNT) bundles supporting Pt. SnO<sub>2</sub>–SWNT bundles were synthesized via chemical-solution route [12]. The addition of Pt onto SnO<sub>2</sub>–SWNT was conducted out by an ethylene glycol reduction method. The Pt/SnO<sub>2</sub>–SWNTs showed enhanced electrocatalytic activity for ethanol oxidation in acid medium, compared to the Pt/SWNT.

By sol–gel method, Pang et al. prepared SnO<sub>2</sub>-carbon nanotubes (CNTs) composites which later were dispersed in H<sub>2</sub>PtCl<sub>6</sub> containing solution to prepare a Pt/SnO<sub>2</sub>-CNT catalyst [16]. The obtained catalyst ink was transferred onto the surface of the graphite electrode followed by coating with a nafion ethanol solution. Comparing with the Pt/SnO<sub>2</sub>/graphite electrode, the Pt/SnO<sub>2</sub>-CNTs/graphite electrode showed better electrochemical performances.

As can be seen from this literature review, it is shown that SnO<sub>2</sub> improves the electrocatalytic performance of Pt towards ethanol oxidation. Note also that the SnO<sub>2</sub>-Pt catalysts have been prepared mostly via chemical routes from mixtures of Pt and SnO<sub>2</sub> precursors and in most case nafion ionomer has been used as a binder. However, the nafion ionomer second role is to increase the three-dimensional zone of catalytic activity (by that increase the performance of Pt catalyst) which is required for electrochemical reaction in the types of design actually used for the catalyst layer in polymer electrolyte fuel cells [17].

This work was undertaken to fabricate free-standing (binderless) Carbon paper (CP)/CNT/SnO<sub>2</sub>/Pt electrodes and investigate their electrocatalytic properties towards ethanol oxidation for instance. Besides the non-use of binders, our electrodes are made of scaled nanostructured films of CNTs, SnO<sub>2</sub> and Pt instead of mixed components [12-16]. In our structures, CNTs are grown by chemical vapor deposition (CVD) onto the Ni-coated CP substrate, whereas SnO<sub>2</sub> and Pt were synthesized by pulsed laser deposition (PLD) technique [18].

The substrate chosen in this work is an untreated CP (Toray) made of 3D network of carbon fibers each having a diameter ranging between 7 and 10 μm. This type of CP is well known in the area of fuel cells as the Gas Diffusion Layer (GDL) in Membrane Electrode Assembly (MEA) and it is highly porous with good electrical conductivity and thus can also act as current collector in the structures developed in this work.

Thus synthesized CNT/SnO<sub>2</sub>/Pt nanostructures are characterized for their surface structure and tested for the oxidation of ethanol, an electrochemical reaction of technological importance in direct ethanol fuel cells (DEFC). We must emphasize that Pt is chosen as a model catalyst for fundamental studies rather than as the best catalyst for the applications considered here.

## 2. EXPERIMENTAL

### 2.1. Carbon nanotubes synthesis

For CNTs growth, a nickel catalyst layer of 5 nm thickness was deposited by pulsed laser deposition (PLD) technique on one side of the CP substrate. This nickel layer was deposited by ablating under vacuum, a pure (99.95%) polycrystalline nickel target with a pulsed KrF excimer laser (wavelength = 248 nm, pulse duration  $\approx$  14 ns, repetition rate of 20 Hz) with a fluence of 5 J cm<sup>-2</sup>. In order to obtain a uniform ablation over the target surface, the target was continuously rotated and translated. The CP substrate was placed at 5 cm from the target and the deposition was performed at room temperature. Afterwards, the CNTs were grown by chemical vapor deposition (CVD) technique. First, the Ni-coated-CP substrate was placed in a horizontal tubular reactor made of quartz tube inserted into a furnace and heated to 700 °C with a 5 °C/min rate under an 50 sccm hydrogen gas (Praxair) flow. When the temperature reached 700 °C, the reactive gas acetylene was introduced simultaneously with argon (Praxair) and H<sub>2</sub> at flow rates of 30, 140 and 100 sccm, respectively. After a synthesis time of 35 min, the acetylene and argon flows were cut off and the furnace cooled down to room temperature under 50 sccm flowing H<sub>2</sub>.

### 2.2. SnO<sub>2</sub> and Pt synthesis

Pt was prepared by PLD by means of a pulsed KrF excimer laser ( $\lambda$  = 248 nm, pulse width = 17 ns, and repetition rate = 50 Hz). Pure platinum (99.99%, Kurt J. Lesker Co.) target was used. A laser fluence of 4 J cm<sup>-2</sup> and 50000 laser pulses were used to deposit the Pt catalyst under 2 Torr of He background pressure. Pure SnO<sub>2</sub> target (99.99%, Kurt J. Lesker Co.) was used to deposit SnO<sub>2</sub> using a laser fluence of 3.5 J cm<sup>-2</sup> and 20000 laser pulses under 2 Torr of He background pressure. Before synthesis, the chamber was evacuated with a turbo pump ( $4 \times 10^{-5}$  Torr). Helium was subsequently introduced in the deposited chamber. The substrate-to-target distance was set at 5 cm.

### 2.3. Material characterization

The surface morphology of the as-synthesized materials was inspected by way of a scanning electron microscope SEM, JEOL, JSM 7401F apparatus and a transmission electron microscopy (JEOL JEM-2100F) operating at 200 kV.

X-ray photoelectron spectroscopy (XPS) measurements were carried out via a VG Escalab 220i-XL set with an Al K $\alpha$  source (1486.6 eV). The anode was operated at 10 kV and 20 mA. The pass energy of the analyzer was fixed at 20 eV. All samples were analyzed with a spot size of 250 $\times$ 1000  $\mu$ m located approximately in the center of the sample. A survey spectra ranging from 0 to 1000 eV was first acquired, and then higher resolution multiplex scan spectra (Pt 4f, Sn 3d, O1s, and C1s core levels) were obtained. The C1s core level peak at 284.6 eV, resulting from hydrocarbon contaminants at the surface, was used as an internal reference. All spectra have been recalibrated with respect to the C1s core level peak of adventitious carbon contamination.

## 2.4. Electrochemical studies

Ethanol oxidation reaction was studied by cyclic voltammetry (CV) and linear sweep voltammetry (LSV) in 0.5 M  $\text{H}_2\text{SO}_4$  and in a mixture of 1 M  $\text{C}_2\text{H}_5\text{OH}+0.5$  M  $\text{H}_2\text{SO}_4$  deaerated solutions. Chronoamperometry was employed for stability evaluation in 1 M  $\text{C}_2\text{H}_5\text{OH}+0.5$  M  $\text{H}_2\text{SO}_4$ . Prior to the electrochemical measurements in ethanol, the surface of the working electrode was cleaned electrochemically by potential cycling in 0.5 M  $\text{H}_2\text{SO}_4$ . Before each test, dissolved oxygen was removed from the solution by bubbling argon for 20 to 30 min. All electrochemical measurements were conducted at room temperature using a three compartments electrochemical cell with the reference electrode and counter electrode being an Ag/AgCl, 3M NaCl and a platinum coil, respectively. The reference electrode was separated from the analyte solution by a Luggin capillary that is very close to the working electrode to minimize the  $IR$  drop. Data acquisition was conducted with a potentiostat/galvanostat Autolab from EcoChemie.

## 3. RESULTS AND DISCUSSIONS

### 3.1. Synthesis and characterization of CNT/SnO<sub>2</sub>

Figures 1a and Fig. 1b show SEM and TEM images of CNTs grown onto the CP substrate, respectively. It can be seen that the carbon microfibers are densely covered by packed wavy aligned arrays of fine and pure CNTs with lengths exceeding tens of micrometers and with an average outer diameter of about 12 nm.

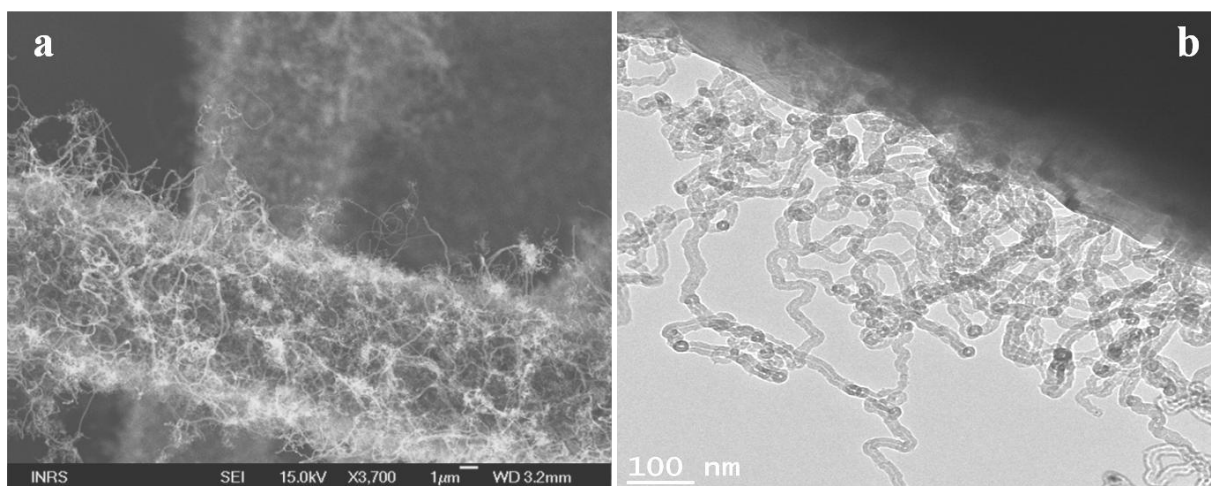


**Figure 1.** Electron microscopy analyses of CVD-synthesized carbon nanotubes onto carbon paper substrate: (a) SEM image and (b) TEM image.

Through Fig. 2a to Fig. 2d are shown SEM images with increasing magnifications of  $\text{SnO}_2$  prepared onto CNTs by PLD under 2 Torr of He. The SEM images of Fig. 2 demonstrate that the

CNTs are highly and uniformly decorated with SnO<sub>2</sub> film displaying a highly porous surface.

TEM analysis of SnO<sub>2</sub> film deposited onto CNTs is reported in Fig. 3. Before going further, we note that our samples are analyzed as-prepared, which means including the CP substrate. It is always challenging to analyze such structures by TEM because of the compactness of the catalysts, the dark underneath carbon paper substrate and the CNTs that move a lot during analysis particularly at the high-resolution analysis. Thus a great deal of efforts and time were taken to obtain the best analyzable TEM images such as these shown in Fig. 3. Thus, Fig. 3a demonstrates an excellent dispersion of uniformly sized and highly interconnected SnO<sub>2</sub> nanoparticles with an average diameter of  $2.9 \pm 1$  nm. Next, a very thorough analysis of the sidewalls of the CNTs with TEM showed that the SnO<sub>2</sub> film is made of columnar nanoparticles (Fig. 3b). An estimation of the SnO<sub>2</sub> film thickness gives a value of ca. 17 nm as depicted in Fig. 3b.

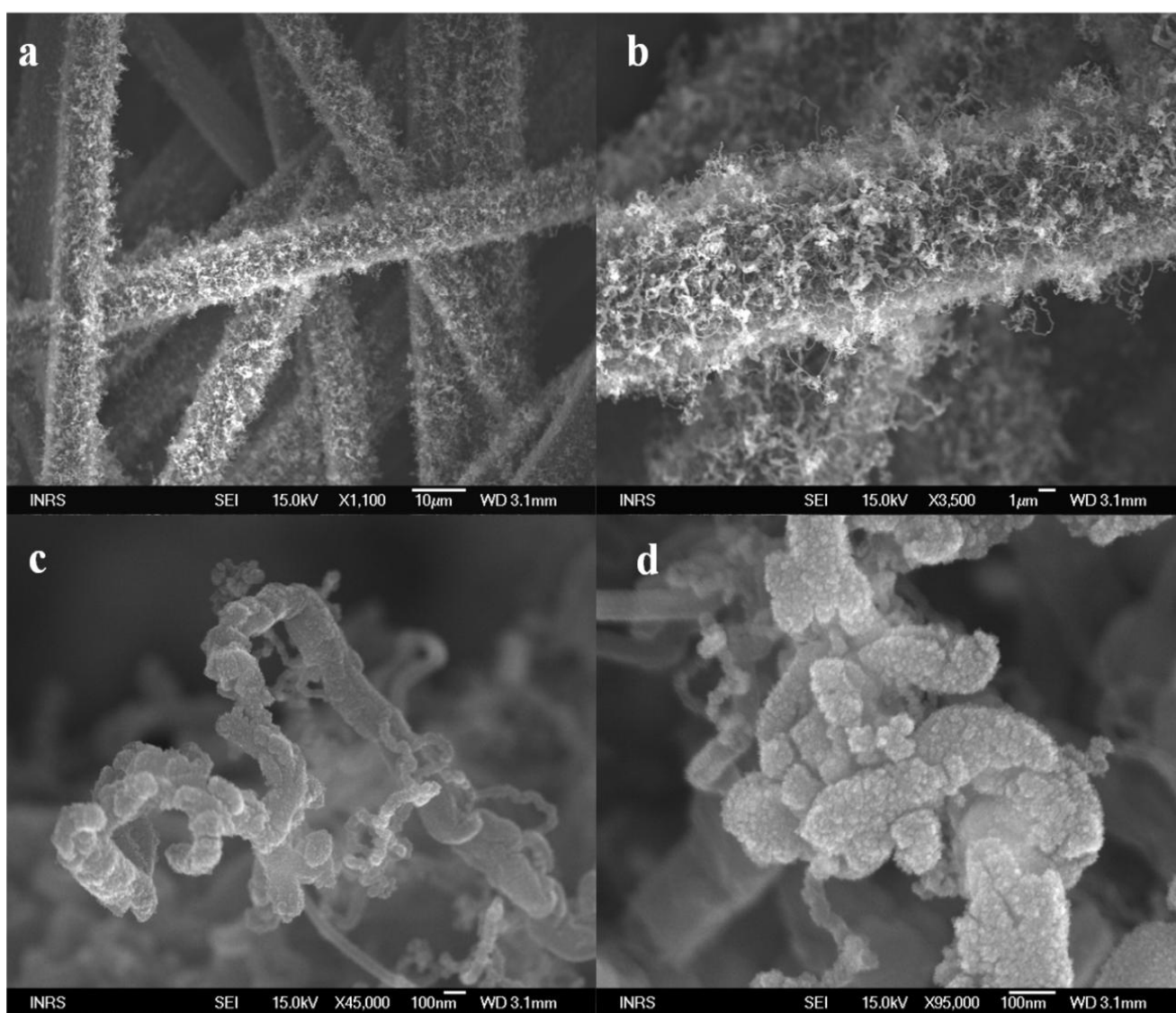


**Figure 2.** SEM images with increasing magnification of PLD-synthesized SnO<sub>2</sub> film onto carbon nanotubes. Magnifications: (a) x1100, (b) x3500, (c) x45000 and (d) x95000.

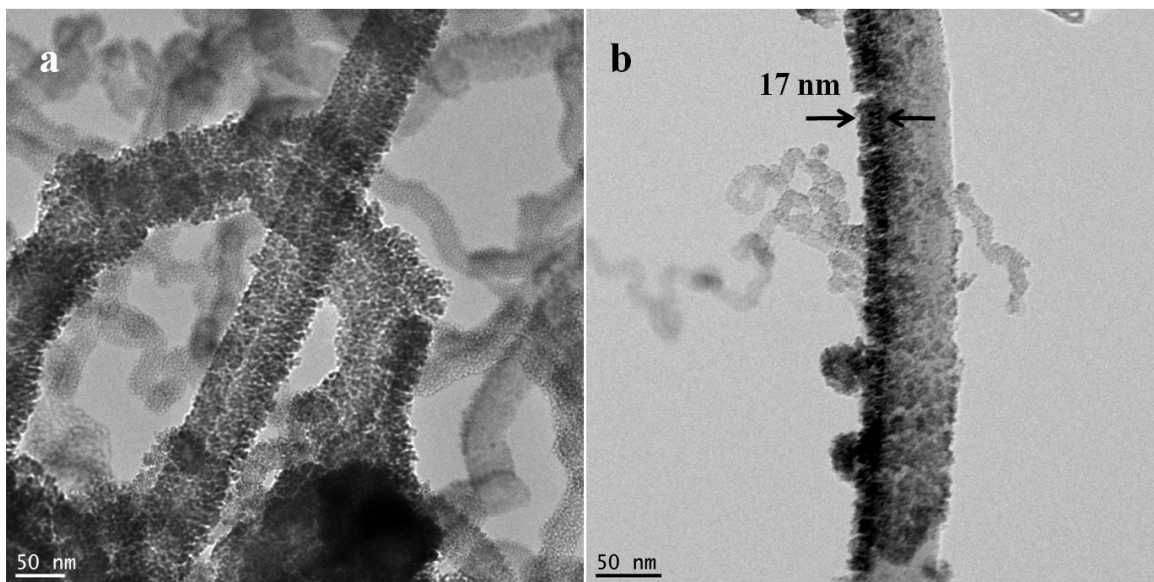


**Figure 3.** TEM images of PLD-synthesized SnO<sub>2</sub> film onto CNTs.

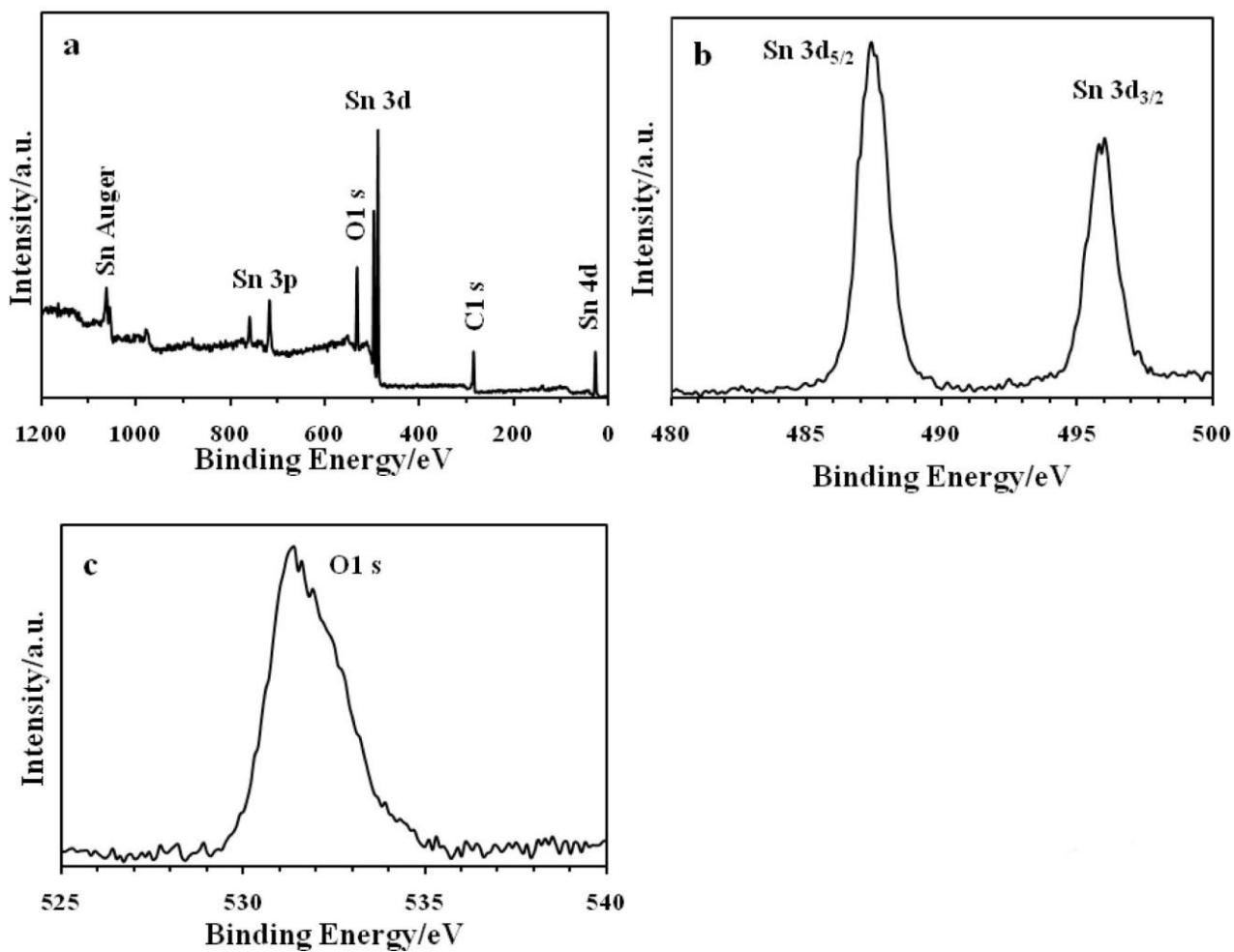


**Figure 4.** X-ray photoelectron spectra of PLD-synthesized SnO<sub>2</sub> film onto CNTs (a) survey spectrum, (b) Sn 3d core level peaks of Sn and (c) O1s core level peak of oxygen.

As can be seen from the images of Fig. 2 and 3, the PLD method is efficient for depositing nano-thin films evenly on both the CNT sidewalls and the ends of the tubes that have not undergone any prior treatment. It is important to note that it is seldom to obtain by other deposition techniques such a highly catalyst decorated CNTs as those obtained in this work. The reason but at the same time a benefit is that during the PLD, the catalyst target is simultaneously rotated and translated across the laser beam to ensure its uniform ablation and in the meantime, this operation ensures an homogeneous deposition over the entire exposed surface of the substrate.

Next, the surface constituent phases of the as-synthesized  $\text{SnO}_2$  ultra-thin film was further confirmed by XPS results shown in Fig. 4. The XPS survey scan (Fig. 4a) presented peaks only for Sn, C and O. The high-resolution XPS Sn 3d and O 1s core level spectra for CNTs-supported  $\text{SnO}_2$  thin film are shown in Fig. 4b and 4c, respectively. The Sn 3d core level spectra show two peaks of which maximum intensities are located at binding energy ( $BE$ ) of 487.4 and 496 eV. The observed binding energy of 487.4 eV is very close to the Sn 3d<sub>5/2</sub> data confirmed in  $\text{SnO}_2$  phase [19]. The O 1s spectrum is composed of one component positioned at around 531.4 eV, which is attributed to O in the  $\text{SnO}_2$  phase.

### 3.2. Synthesis and characterization of CNT/ $\text{SnO}_2$ /Pt

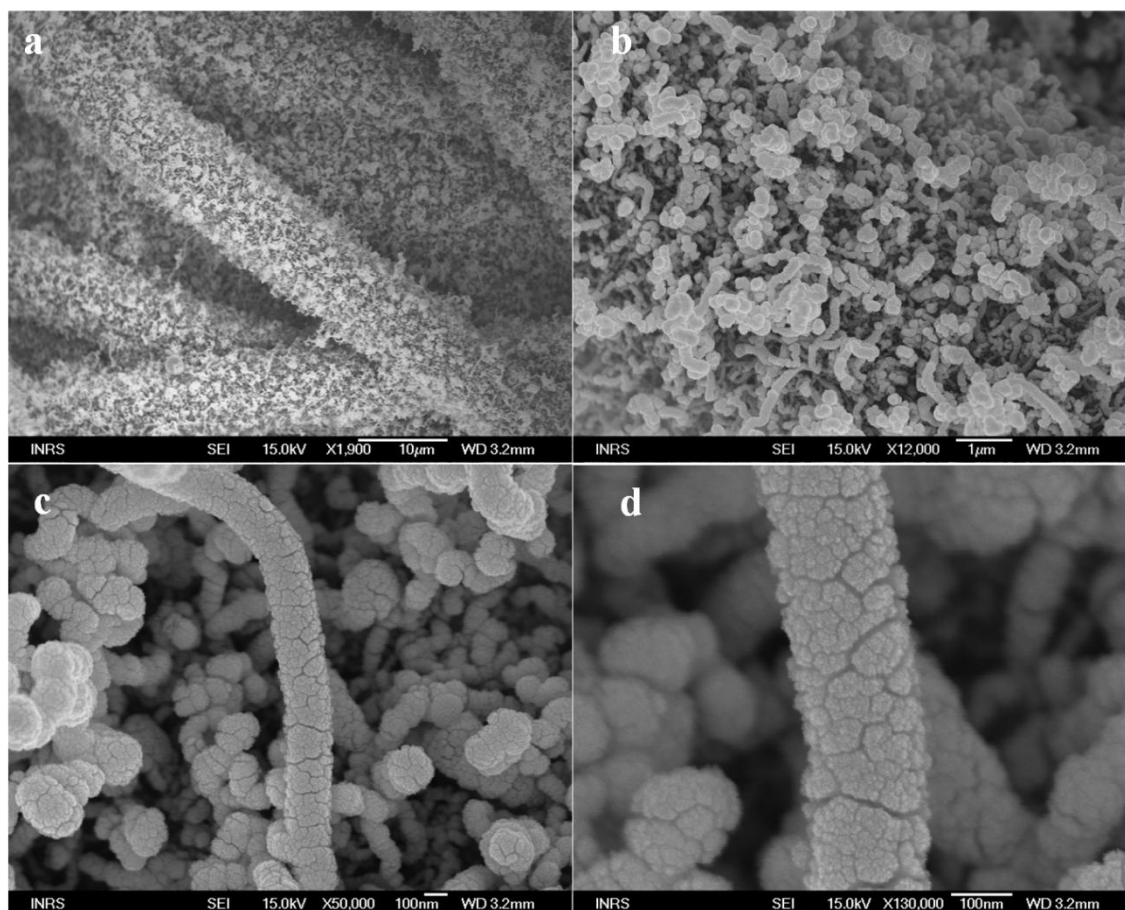


**Figure 5.** SEM images with increasing magnification of PLD-synthesized Pt film onto CNT/ $\text{SnO}_2$ . Magnifications: (a) x1900, (b) x12000, (c) x50000 and (d) x130000.

Figure 5a through Fig. 5d show SEM images with increasing magnifications of Pt film prepared onto CNT/SnO<sub>2</sub>. Pt can clearly be observed densely and highly decorating the CNT/SnO<sub>2</sub> structure. The SEM images show further that the Pt structure possesses a high surface porosity. TEM images of Fig. 6 further confirms the high density and evenness distribution of interconnected nanoparticles of Pt with an average diameter of 3.0 ± 1 nm over CNT/SnO<sub>2</sub> surface (Fig. 6a). Similar to SnO<sub>2</sub> film (Fig. 3b), here too the Pt film assembles into columnar nanoparticles as demonstrated in Fig. 6b. The Pt film thickness estimated from TEM (as illustrated in Fig. 6b) is about 40 nm.

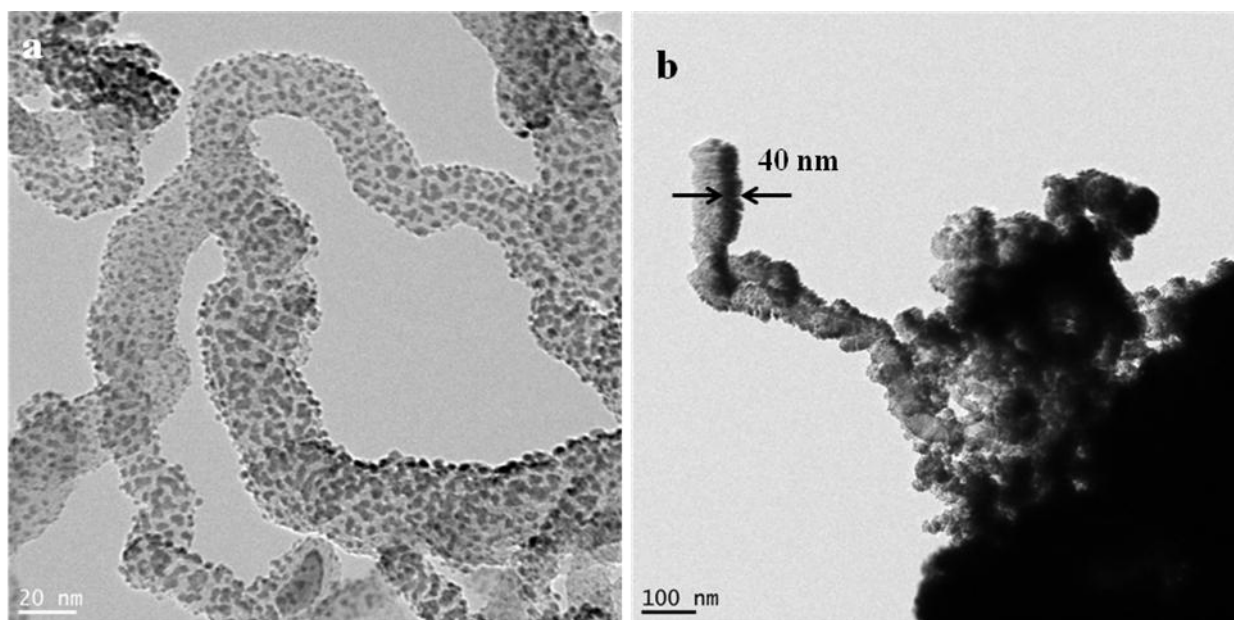


Figure 6. TEM images of PLD-synthesized Pt film onto CNT/SnO<sub>2</sub>.

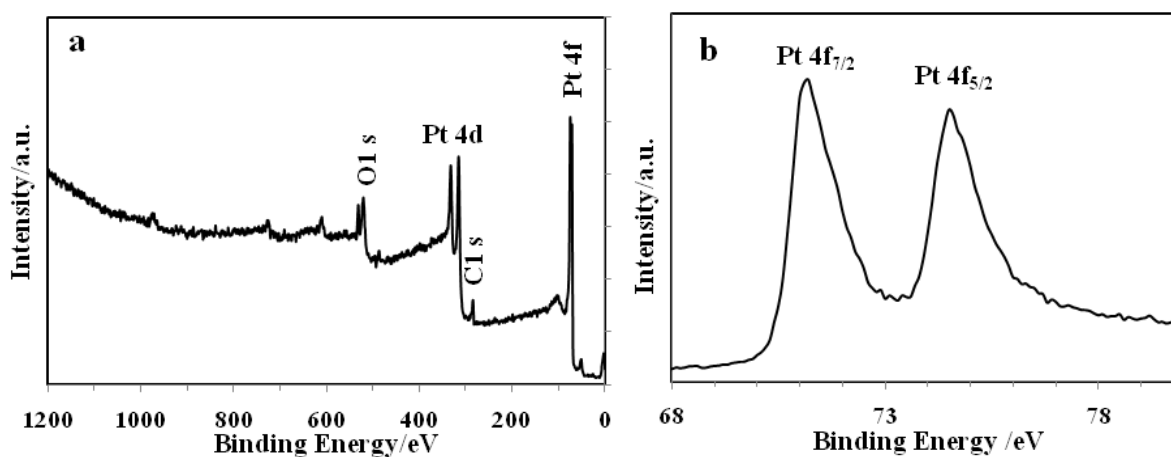
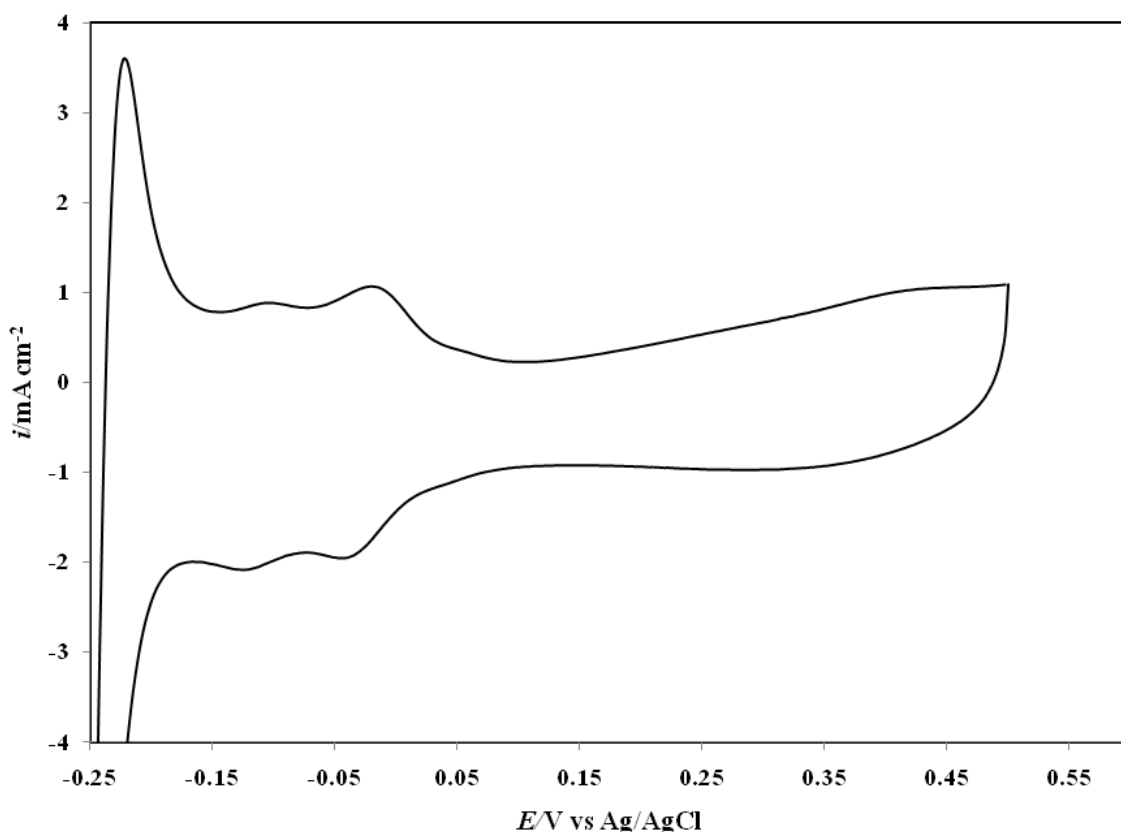


Figure 7. X-ray photoelectron spectra of PLD-synthesized Pt film onto CNT/SnO<sub>2</sub> (a) survey spectrum and (b) Pt 4f core level peaks.

XPS survey scans (Fig. 7a) conducted at the surface of CNT/SnO<sub>2</sub>/Pt structures showed peaks just for Pt, C and O and no peak related to Sn, indicating that Pt film fully coated the beneath SnO<sub>2</sub> layer. The high-resolution XPS Pt 4f core level spectrum exhibits two peaks whose maximum intensities are positioned between 71.2 and 74.5 eV binding energy range (Fig. 7b) in accordance with Pt being in a metallic state [20].

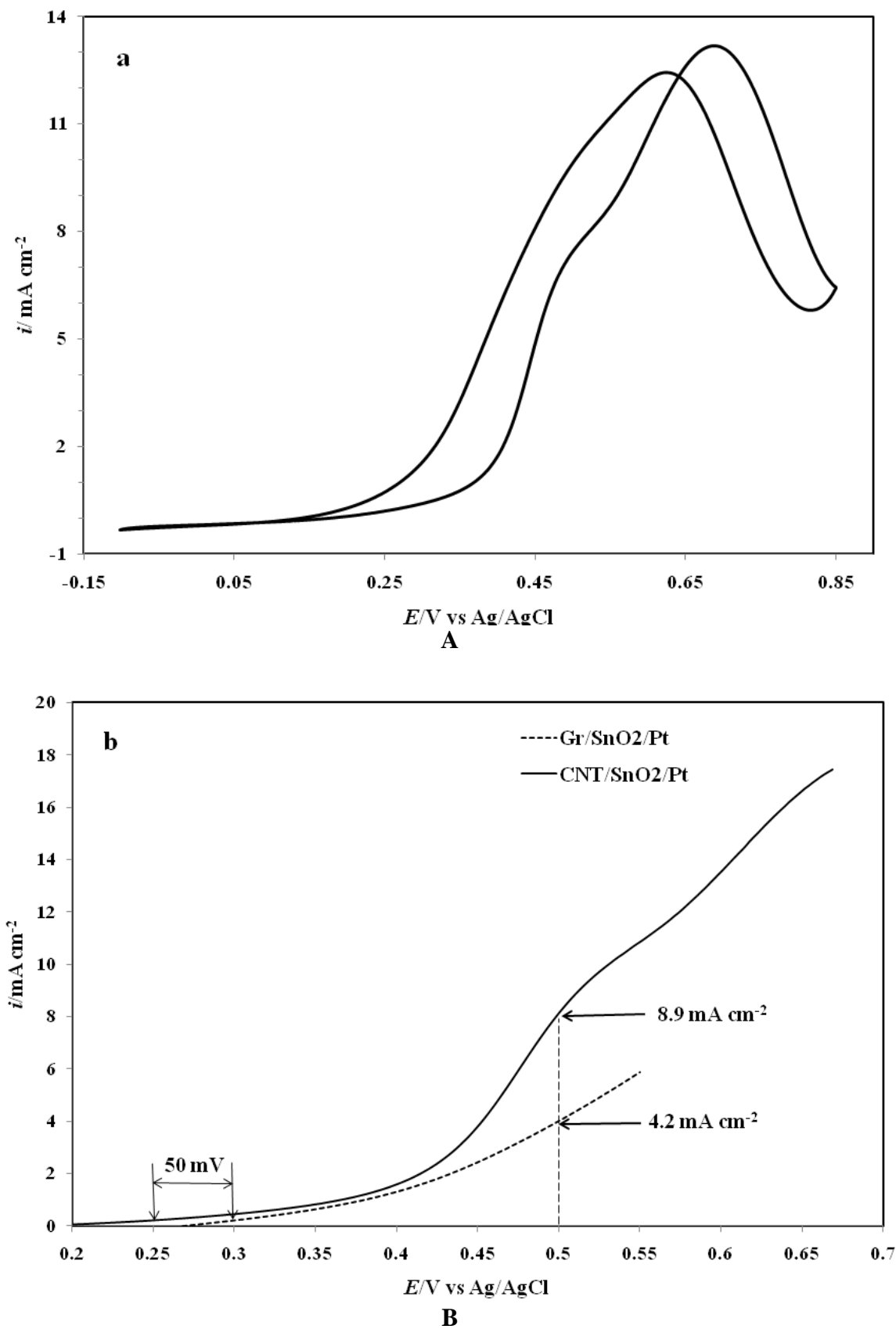
### 3.3. Electrocatalytic properties

Figure 8 corresponds to cyclic voltammetry (CV) experiment run at CNT/SnO<sub>2</sub>/Pt electrode in 0.5 M H<sub>2</sub>SO<sub>4</sub> deaerated solution.



**Figure 8.** Cyclic voltammetry in 0.5 M H<sub>2</sub>SO<sub>4</sub> solution with the scan rate of 50 mV s<sup>-1</sup> recorded at CNT/SnO<sub>2</sub>/Pt electrode.

The CV was recorded by setting the anodic limit to 0.50 V to avoid the leaching of tin that occurs at more positive potential in sulfuric acid solution [21-23]. As can be seen from Fig. 8, the CNT/SnO<sub>2</sub>/Pt electrode exhibits the very well-known several hydrogen adsorption (H<sub>ads</sub>) and desorption (H<sub>des</sub>) peaks in the potential region of ca. 0.1 to -0.2 V vs Ag/AgCl which indicates the contributions of various Pt (*hkl*) facets [23-25].



**Figure 9.** Voltammetry in 0.5 M H<sub>2</sub>SO<sub>4</sub>+ 1 M C<sub>2</sub>H<sub>5</sub>OH solution. (a) CV at CNT/SnO<sub>2</sub>/Pt electrode with the scan rate of 2 mV s<sup>-1</sup>, and (b) comparative linear sweep voltammograms of CNT/SnO<sub>2</sub>/Pt and Gr/SnO<sub>2</sub>/Pt with the scan rate of 5 mV s<sup>-1</sup>.

Figure 9a shows quasi-steady state CV with  $2 \text{ mV s}^{-1}$  potential scan rate at the CNT/SnO<sub>2</sub>/Pt electrode recorded in a 0.5 M H<sub>2</sub>SO<sub>4</sub>+1 M C<sub>2</sub>H<sub>5</sub>OH solution. Well defined characteristic ethanol oxidation waves are obtained in good agreement with the literature [23, 26]. The forward anodic peak is located at 0.66 V vs Ag/AgCl with a current density of  $13 \text{ mA cm}^{-2}$  which is quite high at such low potential scan rate. For comparison, SnO<sub>2</sub>/Pt structure was synthesized onto a smooth disk of graphite (Gr) using PLD conditions similar to SnO<sub>2</sub>/Pt onto CNTs. The electrocatalytic behaviour of the Gr/SnO<sub>2</sub>/Pt electrode towards ethanol oxidation is compared with that of CNT/SnO<sub>2</sub>/Pt electrode with the linear sweep voltammograms (LSVs) shown in Fig. 9b.

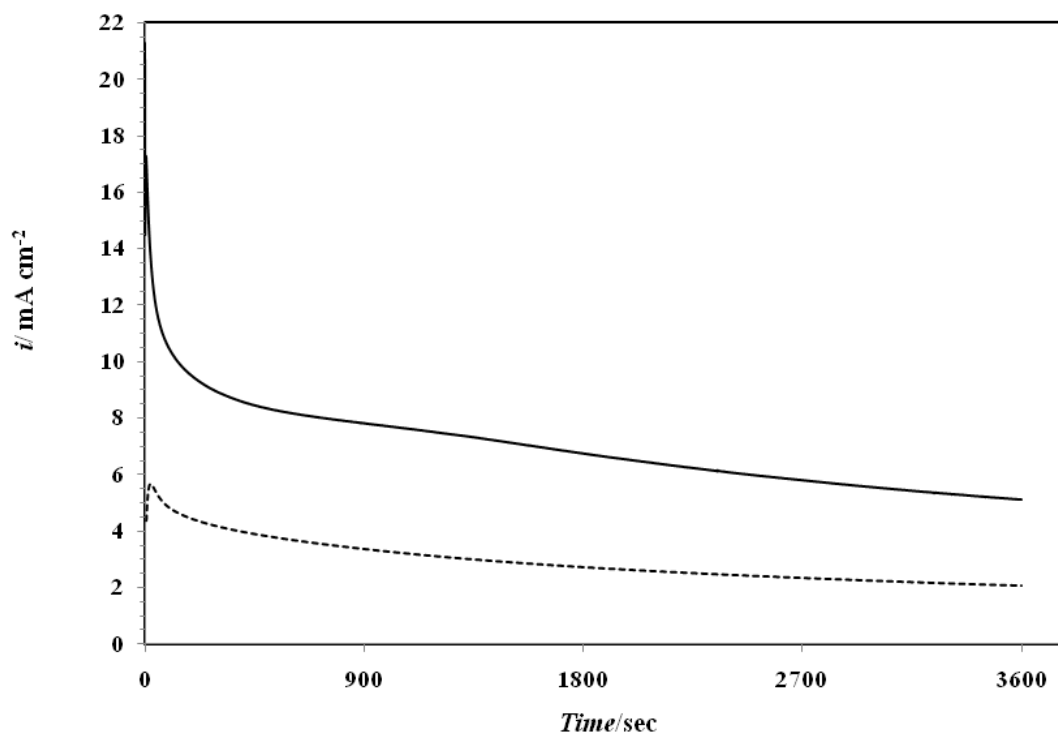


**Figure 10.** Chronoamperometric curves at CNT/SnO<sub>2</sub>/Pt electrode recorded in 0.5 M H<sub>2</sub>SO<sub>4</sub>+ 1 M C<sub>2</sub>H<sub>5</sub>OH solution at two applied potentials: 0.5 V (dashed line), and 0.6 V vs Ag/AgCl (full line).

Clearly considerably higher kinetics towards ethanol electro-oxidation are observed with the CNT/SnO<sub>2</sub>/Pt electrode. Indeed, as depicted in Fig. 9b, two comparative parameters that indicate about the rate of an electrochemical reaction were extracted from the LSVs; namely the current density at a fixed potential (0.5 V vs Ag/AgCl) and the onset potential for ethanol oxidation that is defined here as the potential value at which the anodic current (current due to ethanol oxidation) starts to flow. At the potential of 0.5 V, the CNT/SnO<sub>2</sub>/Pt electrode delivered a current density of  $8.9 \text{ mA cm}^{-2}$  that is 2.1 times higher than the corresponding activity of Gr/SnO<sub>2</sub>/Pt electrode ( $4.2 \text{ mA cm}^{-2}$ ). In addition, the electron-transfer kinetics at the CNT/SnO<sub>2</sub>/Pt has been fostered compared to a Gr/SnO<sub>2</sub>/Pt surface as demonstrated by the decreased

overpotential required to oxidize ethanol. Indeed, the CNT/SnO<sub>2</sub>/Pt electrode showed the lowest onset potential value of 0.25 V that is 50 mV negative than that displayed by the Gr/SnO<sub>2</sub>/Pt electrode. These observations are qualitatively in line with the findings of Pang et al. who reported enhanced ethanol electro-oxidation at Pt/SnO<sub>2</sub>-CNTs/Gr composites when compared to Pt/SnO<sub>2</sub>/Gr composites electrodes [16]. The authors ascribed such enhancement to the contribution of two parameters. The first is the diameter of SnO<sub>2</sub> particles in the SnO<sub>2</sub>-CNT composites was smaller than that in pure SnO<sub>2</sub> and that resulted in more active sites on the former electrode. The second parameter was due to the high electrical conductivity of CNTs. For our conditions, the particle size effect can be ruled out because Pt and SnO<sub>2</sub> were prepared with the same conditions of PLD either onto graphite or onto CNTs. The enhanced behavior observed in our work is due to the unique electrical properties of CNTs which enhance the conductivity of the CNT/SnO<sub>2</sub>/Pt electrode and by that promotes the electron transfer reactions but also to the morphology of the CNTs which confers an excellent platform for supporting, dispersion and utilization of the SnO<sub>2</sub> catalyst better than smooth graphite.

Next, chronoamperometric curves were recorded to check the long-term activity and stability of the CNT/SnO<sub>2</sub>/Pt electrode. This was done by stepping the potential from the open circuit potential to 0.5 V and 0.6 vs Ag/AgCl in 0.5 M H<sub>2</sub>SO<sub>4</sub>+1 M C<sub>2</sub>H<sub>5</sub>OH. The current density values were recorded for 1 hour, and the resulting current density-time (*i-t*) curves are shown in Fig. 10. Both *i-t* responses displayed an initial fast decay followed by a slower decrease upon long-time operation, attaining a quasi-equilibrium steady state. The fast decaying part is attributed to the rapid increase of the surface coverage by intermediate species, such as adsorbed CO during ethanol oxidation reaction. The results of Fig. 10 confirm the good activity and stability of the CNT/SnO<sub>2</sub>/Pt electrocatalyst. The steady state current density of 5.15 mA cm<sup>-2</sup> delivered at 0.6 V is about 2.6 times higher than the one delivered 0.5 vs Ag/AgCl (2 mA cm<sup>-2</sup>).

#### 4. CONCLUSIONS

Nano-thin films of SnO<sub>2</sub>/Pt have been synthesized for the first time onto CNTs by means of pulsed laser deposition technique. For the experimental deposition conditions used here films of 17 nm and 40 nm thicknesses were obtained for SnO<sub>2</sub> and Pt, respectively.

In this work, Pt is chosen as a model catalyst for fundamental studies rather than as the best catalyst for the applications considered here. Thus, the CNT/SnO<sub>2</sub>/Pt electrode developed here responded well when used as an anode, i.e., it exhibited good electrocatalytic activity and stability towards ethanol oxidation better than the Gr/SnO<sub>2</sub>/Pt electrode. There is still room for improvement of the SnO<sub>2</sub> contribution to ethanol oxidation. Such improvement is being sought in our laboratory by varying the effect of the SnO<sub>2</sub> thickness but also the influence of its surface morphology smooth vs porous.

Another variant that deserves to be studied is the use of the PLD to co-deposit SnO<sub>2</sub> and Pt onto CNTs. It would be interesting from a fundamental point of view to compare the electrocatalytic performance of such structures not only versus the one developed in this work but also against those

prepared from mixtures of SnO<sub>2</sub> and Pt previously reported in the literature. Such work is under research and development to use the cross-beam laser deposition (dual beam) to co-deposit nanostructured SnO<sub>2</sub> and Pt onto CNTs.

#### ACKNOWLEDGEMENT

This work was supported by the Natural Sciences Engineering Research Council of Canada (NSERC), the Centre Québécois sur les Matériaux Fonctionnels (CQMF) and the MDEIE.

#### References

1. Y.S. He, J.C. Campbell, R.C. Murphy, M.F. Arendt and J.S. Swinnea, *J. Mater. Res.* 8 (1993) 3131.
2. A.Z. Adamyan, Z.N. Adamyan, V.M. Aroutiounian, *Int. J. Hydrogen Energy* 34 (2009) 8438.
3. G. Zhang, M. Liu, *Sens. Actuators B* 69 (2000) 144.
4. Z. Peng, Z. Shi and M. Liu, *Chem. Commun.* (2000) 2125.
5. R.K. Selvan, I. Perelshtein, N. Perkas, and A. Gedanken, *J. Phys. Chem. C* 112 (2008) 1825.
6. S. Abanades, P. Charvin, F. Lemont, G. Flamant, *Int. J. Hydrogen Energy* 33 (2008) 6021.
7. S. Ferrere, A. Zaban, and B.A. Gregg, *J. Phys. Chem. B* 101 (1997) 4490.
8. Y. Chen, J. Wang, X. Meng, Y. Zhong, R. Li, X. Sun, S. Ye, S. Knights, *Int. J. Hydrogen Energy* (2011) doi:10.1016/j.ijhydene.2011.05.156.
9. X. Zhang, H. Zhu, Z. Guo, Y. Wei, F. Wang, *Int. J. Hydrogen Energy* 35 (2010) 8841.
10. A.O. Neto, M. Brandalise, R.R. Dias, J.M.S. Ayoub, A.C. Silva, J.C. Penteado, M. Linardi E.V. Spinacé, *Int. J. Hydrogen Energy* 35 (2010) 9177.
11. L. Jiang, L. Colmenares, Z. Jusys, G.Q. Sun, R.J. Behm, *Electrochim. Acta* 53 (2007) 377.
12. R.S. Hsu, D. Higgins, Z. Chen, *Nanotechnology* 21 (2010) 165705.
13. E. Higuchi, K. Miyata, T. Takase, H. Inoue, *J. Power Sources* 196 (2011) 1730.
14. H. Zhang, C. Hu, X. He, L. Hong, G. Du, Y. Zhang, *J. Power Sources* 196 (2011) 4499.
15. G.R. Salazar-Banda, H.B. Suffredini, L.A. Avaca, S.A.S. Machado, *Mater. Chem. Phys.* 117 (2009) 434.
16. H.L. Pang, J.P. Lu, J.H. Chen, C.T. Huang, B. Liu, X.H. Zhang, *Electrochim. Acta* 54 (2009) 2610.
17. G. Sasikumar, J.W. Ihm, H. Ryu, *Electrochim. Acta* 50 (2004) 601.
18. D.B. Chrisey, G.K. Hübner, *Pulsed Laser Deposition of Thin Films*, Wiley, New York (1994).
19. J. Luo, C. Xu, *J. Non-Cryst Solids* 119 (1990) 37.
20. C.D. Wagner, W.M. Riggs, L.E. Davis, J.F. Moulder, *Handbook of X-ray Photoelectron Spectroscopy*, G.E. Muilenberg, Perkin-Elmer Corp Eden Prairie MN USA (1979).
21. G. Siné, G. Fóti, Ch. Comninellis, *J. Electroanal. Chem.* 595 (2006) 115.
22. L. Colmenares, H. Wang, Z. Jusys, L. Jiang, S. Yan, G.Q. Sun, R.J. Behm, *Electrochim. Acta* 52 (2006) 221.
23. H. Wang, Z. Jusys, R.J. Behm, *J. Power Sources* 154 (2006) 351.
24. K. Kinoshita, D.R. Ferrier, and P Stonehart, *Electrochim. Acta* 23 (1978) 45.
25. T.J. Schmidt, H.A. Gasteiger, G.D. Stab, P.M. Urban, D.M. Kolb, and R.J. Behm, *J. Electrochem. Soc.* 145 (1998) 2354.
26. T. Iwasita and E. Pastor, *Electrochim. Acta* 39 (1994) 531.